# Magnetization Process in Vortex-imprinted $Ni_{80}Fe_{20}/Ir_{20}Mn_{80}$ Square Elements

**H. Xu[1], J. Kolthammer[1], J. Rudge[1], E. Girgis[1]\*, B. C. Choi[1]\*\*,**
**Y. K. Hong[2], G. Abo[2], Th. Speliotis[3], and D. Niarchos[3]**

*[1]Dept. of Physics and Astronomy, University of Victoria, Victoria, BC, V8P 5C2, Canada*
*[2]Dept. of Electrical and Computer Engineering, The University of Alabama, Tuscaloosa, AL 35487, USA*
*[3]Institute of Materials Science, NCSR "Demokritos," 15310 Aghia Paraskevi, Greece*

The vortex-driven magnetization process of micron-sized, exchange-coupled square elements with composition of $Ni_{80}Fe_{20}$ (12 nm)/$Ir_{20}Mn_{80}$ (5 nm) is investigated. The exchange-bias is introduced by field-cooling through the blocking temperature ($T_B$) of the system, whereby Landau-shaped vortex states of the $Ni_{80}Fe_{20}$ layer are imprinted into the $Ir_{20}Mn_{80}$. In the case of zero-field cooling, the exchange-coupling at the ferromagnetic/anti-ferromagnetic interface significantly enhances the vortex stability by increasing the nucleation and annihilation fields, while reducing coercivity and remanence. For the field-cooled elements, the hysteresis loops are shifted along the cooling field axis. The loop shift is attributed to the imprinting of displaced vortex state of $Ni_{80}Fe_{20}$ into $Ir_{20}Mn_{80}$, which leads to asymmetric effective local pinning fields at the interface. The asymmetry of the hysteresis loop and the strength of the exchange-bias field can be tuned by varying the strength of cooling field. Micromagnetic modeling reproduces the experimentally observed vortex-driven magnetization process if the local pinning fields induced by exchange-coupling of the ferromagnetic and antiferromagnetic layers are taken into account.

Keywords : exchange bias, vortex magnetization, magneto-optics, micromagnetic modeling

## 1. Introduction

The magnetic properties of exchange-coupled ferromagnetic (FM)/antiferromagnetic (AFM) structures have been the subject of considerable research as of late, motivated by both the fundamental interest at reduced dimensions and potential applications in high-density magnetic storage and spintronic logic devices [1-5]. Patterned square and disk elements are of particular interest, owing to their well-defined remanent magnetic vortex states, with a number of studies focusing on both the quasi-static magnetization reversal and non-equilibrium magnetization processes [6-12]. When a FM/AFM bilayer system is heated past the blocking temperature, $T_B$, and subsequently cooled, the interface exchange interaction causes the interfacial spins of the AFM and FM layers to align, imprinting the magnetization configuration of the FM layer into the

AFM. This imprinting manifests itself as a unidirectional anisotropy and a shift in the magnetic hysteresis curve [1]. This phenomenon is known as exchange-bias [13, 14]. Previous studies on the magnetization reversal of circular FM/AFM bilayer disks have shown that cooling through the blocking temperature of the system in a non-saturating external field allows the imprinting of the displaced vortex magnetization structures into the AFM [10, 11, 15]. The resulting magnetization reversal curve exhibits characteristic vortex hysteresis with added asymmetry controlled by the cooling field. In this paper, we investigate the magnetization reversal of micron-sized, exchange-biased FM/AFM bilayer square elements under varying cooling field strengths. The resulting hysteresis loops retain the characteristic shape of a shifted vortex hysteresis as a result of the exchange bias, with additional complexity due to the Landau magnetic remanent state of the square elements.

## 2. Experimental Details

Arrays of $10\,\mu m \times 10\,\mu m$ elements with the layer configuration of $Ir_{20}Mn_{80}(5\,nm)/Ni_{80}Fe_{20}(12\,nm)/Ta(5\,nm)$

---

*Permanent Address: Advanced Materials and Nanotechnology Lab, National Research Centre, 12622 Dokki, Giza, Egypt.
**Corresponding author: Tel: +1-250-721-7731
Fax: +1-250-721-7731, e-mail: bchoi@uvic.ca

were fabricated on 50 µm-thick glass substrates via electron-beam lithography and DC-triode sputter deposition. After fabrication, the samples were heated to 600 K, above the blocking temperature of the system, and subsequently cooled to room temperature in the presence of constant in-plane cooling fields ($H_{CF}$) of 0 Oe, 15 Oe and 40 Oe. This process manipulates the remanent magnetization configuration of $Ni_{80}Fe_{20}/Ir_{20}Mn_{80}$ square elements, and introduces an exchange-bias effect to the system. Detailed micromagnetic simulations [16] were performed to understand the magnetization process observed in experiments. A square element with the size of 2 µm × 2 µm × 20 nm was divided into unit cells of 10 $nm^3$. Note that the size of the modeled element is smaller than the real sample to keep the computation time within reasonable limits. The AFM layer itself was not directly included in the modeling, instead, the exchange-bias at the FM/AFM interface was represented through a position-dependent field of magnitude 90 Oe pinned at the bottom layer of the ferromagnet [8, 15]. The material parameters used for $Ni_{80}Fe_{20}$ are: saturation magnetization $M_s$=800 emu/$cm^3$, exchange stiffness constant $A$=1.05 × $10^{-6}$ erg/cm, and uniaxial magnetic anisotropy $K_u$=1000 erg/$cm^3$ along the $x$–direction (Fig. 4). A symmetric vortex initial state was relaxed in the presence of an in-plane uniform field equal to $H_{CF}$ without exchange-interaction with the AFM, resulting in a displaced vortex state. The position-dependent pinning field was constructed from this modified vortex state of the FM element subject to the desired $H_{CF}$.

## 3. Results and Discussion

Fig. 1 shows the longitudinal hysteresis curves measured using magneto-optical Kerr effect (MOKE) at room temperature, in which the elements were subject to a ±100 Oe, 1 Hz sweeping field along the $H_{CF}$ axis. The laser beam is focused on a spot of Ø ≈ 20 µm, and the MOKE signal measures the change of the in-plane magnetization from an individual element. First, the magnetic properties for the reference sample (12 nm thick single layer $Ni_{80}Fe_{20}$ square) (a) and the zero-field cooled (ZFC, i.e., $H_{CF}$ = 0 Oe) $Ni_{80}Fe_{20}/Ir_{20}Mn_{80}$ element (b) are compared. In both cases, the loops reveal the constricted central portion, which is a typical feature of the vortex-mediated magnetization process [8, 10, 14]. For the reference sample, a vortex state emerges at the nucleation field $H_N$ (= 8 Oe) when the magnetic field is decreased from saturation, whereupon the average magnetization of the element decreases abruptly. The finite values of coercivity $H_C$ and remanence $M_R$ are attributed to the imperfection of the square shape and the presence of the non-negligible
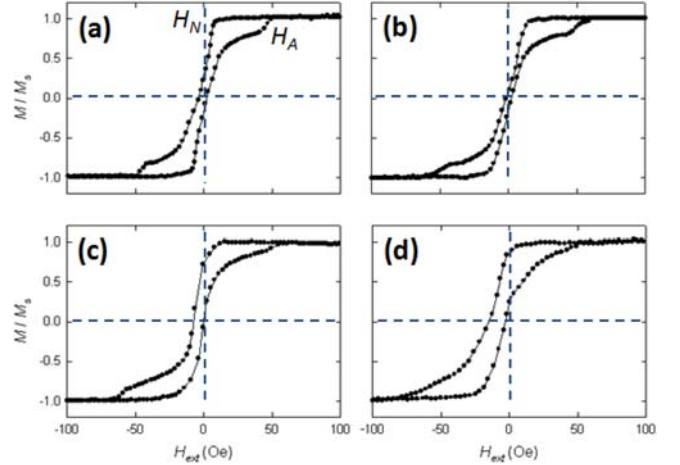


**Fig. 1.** MOKE hysteresis curves for the reference (12 nm thick $Ni_{80}Fe_{20}$) (a) and exchange-biased $Ni_{80}Fe_{20}/Ir_{20}Mn_{80}$ square elements prepared in the presence of 0 Oe (b), 15 Oe (c), and 40 Oe (d) cooling fields. The magnetization reversal of all samples occurs via vortex nucleation/annihilation. The hysteresis curves for field-cooled elements exhibit asymmetry and are shifted along the magnetic field axis due to the exchange-bias effect.

magnetic anisotropy induced during the $Ni_{80}Fe_{20}$ layer deposition. The disappearance of the vortex core occurs at the annihilation field $H_A$ (=50 Oe). For the ZFC element (b), the overall magnetization process is almost identical to that of the $Ni_{80}Fe_{20}$ reference sample (a). $H_N$ and $H_A$ values for the ZFC element are measured at 15 Oe and 62 Oe, respectively, which are substantially greater than those obtained from the reference sample. Furthermore, the coercivity and remanence are decreased for the ZFC $Ni_{80}Fe_{20}/Ir_{20}Mn_{80}$ element. These observations suggest that the magnetic stability of the vortex state is enhanced for the ZFC $Ni_{80}Fe_{20}/Ir_{20}Mn_{80}$ element compared to the $Ni_{80}Fe_{20}$ reference sample, which is in agreement with the previous report by Sort *et al.* [8]. The stability enhancement is attributed to the vortex-imprinting of the AFM layer giving rise to a central "restoring" force, as a result of the symmetric pinning field, which acts on the displaced vortex core. This implies that the exchange-coupling at the FM/AFM interface prescribes a favorable low energy path for the magnetization process, dictated by the imprinted vortex state in the AFM. A lower-bound estimate of the strength of this exchange-coupling effect can be determined from the increase in annihilation field $H_A$ from the reference sample to the ZFC element [17, 18], which in our case is 12 Oe. The vortex magnetization configurations as the remanent states of the 12 nm $Ni_{80}Fe_{20}$ reference sample (a) and ZFC $Ni_{80}Fe_{20}/Ir_{20}Mn_{80}$ element (b) are confirmed by scanning Kerr microscope measurements (Fig. 2). The contrasts in the images reflect the local magnetization
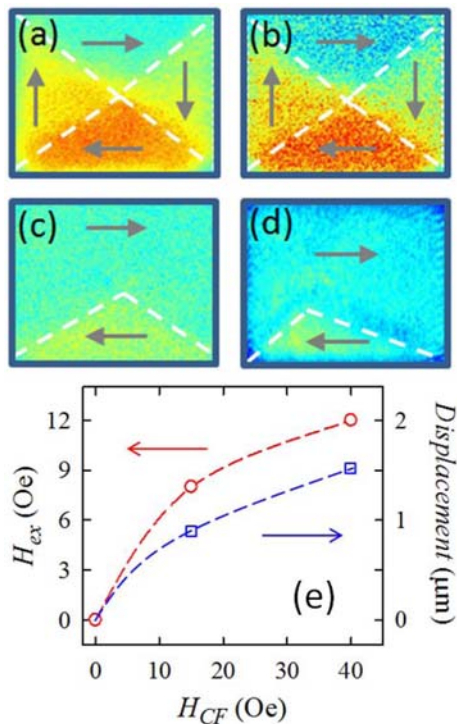
**Fig. 2.** Magnetization configurations for the reference (12 nm thick $Ni_{80}Fe_{20}$) (a) and exchange-biased $Ni_{80}Fe_{20}/Ir_{20}Mn_{80}$ square elements prepared in the presence of 0 Oe (b), 15 Oe (c), and 40 Oe (d) cooling fields. The contrasts in the images reflect the local magnetization direction, as indicated by the arrows. The vortex core cannot be resolved experimentally, but rather implied through the contrast between the domain walls. The zero-field cooled sample (a) supports a symmetric fluxed-closed Landau-type structure with a central vortex, while the field-cooled samples, (c) and (d), reveal displaced vortex structure as remanent states. (e) Cooling field dependence of $H_{ex}$ (o) and the vortex core position at remanence ($\square$) measured from the domain images (b)-(d). The dotted lines are guides to the eye.

direction, as indicated by the arrows. The vortex core cannot be resolved experimentally, but rather implied through the contrast between the domains. The domain image shown in Fig. 2(b) clearly demonstrates that the ZFC FM/AFM square element supports a symmetric Landau structure as the remanent state.

Significant modifications in the remanent magnetization configurations are observed for the field-cooled elements. Fig. 2(c) and (d) show the scanning Kerr microscope images for the $Ni_{80}Fe_{20}/Ir_{20}Mn_{80}$ elements, which are field cooled with $H_{CF}$ of 15 and 40 Oe, respectively, showing vortex-shifted asymmetric Landau vortex configurations at remanence. Fig. 1(c) and (d) show the corresponding hysteresis measurements. The field-cooled samples retain the characteristics of vortex hysteresis, while exhibiting evident shifts of the hysteresis curve along the cooling
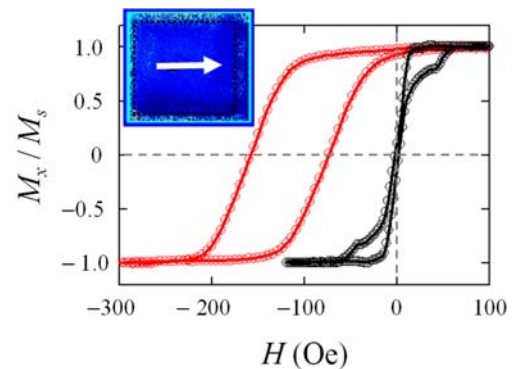


**Fig. 3.** $H_{ex}$ of 120 Oe is measured by saturating the FM/AFM bilayer square element with a large uniform field during cooling ($H_{CF}$=500 Oe). Magnetization reversal without vortex nucleation is observed, with a large shift in the hysteresis loop (red curve). Hysteresis curve prepared in $H_{CF}$=0 Oe is also shown for comparison (black curve).

field direction. The exchange-bias field ($H_{ex}$), estimated from the hysteresis loop-shift, is found to increase with increasing $H_{CF}$. The dependence of $H_{ex}$ on $H_{CF}$ is attributed to the increasing displacement of the vortex core from its central position as $H_{CF}$ becomes higher, as shown in Fig. 2(c)-(d). The offset of the remanent vortex state consequently leads to hysteresis loop shift, marked asymmetry in the hysteresis loop, modification of the vortex nucleation and annihilation fields, and increases in remanence and coercivity [15]. Fig. 2(e) shows the cooling field dependence of $H_{ex}$ and vortex core displacement at remanence, measured from the centre of the domain images in Fig. 2(b)-(d). A clear correlation of $H_{ex}$ and the displacement of the vortex core can be seen. We note that the vortex-mediated magnetization process is no longer observed when the cooling field, $H_{CF}$, exceeds the saturating field of $Ni_{80}Fe_{20}$. As demonstrated by the hysteresis loop (red curve) in Fig. 3, the imprinting of the saturated magnetization state of $Ni_{80}Fe_{20}$ into the antiferromagnet for $H_{CF}$=500 Oe leads to an $H_{ex}$ of 120 Oe, a prescription for achieving large exchange-bias effect.

The equilibrium magnetic configurations simulated for various $H_{CF}$ are shown in the upper panel of Fig. 4. As shown in Fig. 4(a)-(c), the increase of the cooling field strength expands the domain magnetized in the direction of the applied magnetic field, deforming the symmetric Landau vortex structure. Consequently, the vortex core is pushed away from the centre of the square element, and vortex-shifted asymmetric Landau configurations are energetically more favorable, as shown in Fig. 4(b). At a very high $H_{CF}$, e.g. Fig. 4(c), the remanent magnetization shows a displaced vortex state close to saturation. The energies numerically obtained from the symmetric and deformed
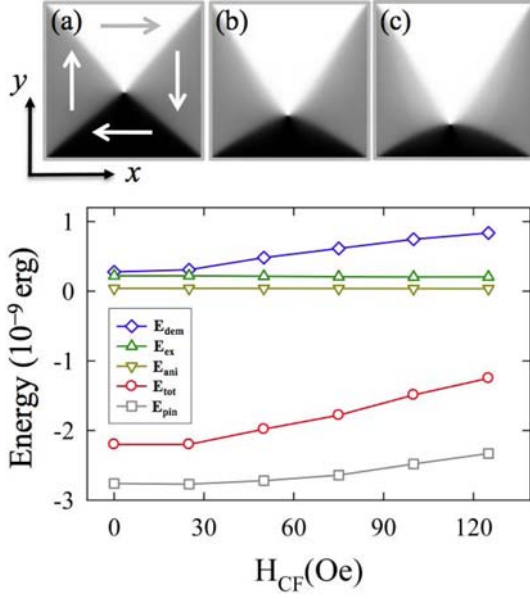
**Fig. 4.** (*top panel*) Magnetization configurations at remanence simulated for various cooling field strength: (a) $H_{CF}=25$ Oe, (b) $H_{CF}=75$ Oe, and (c) $H_{CF}=125$ Oe. For high $H_{CF}$ (c), a displaced remanent Landau vortex state close to saturation is obtained. (*bottom panel*) Energies are plotted as a function of cooling field $H_{CF}$. The values are numerically obtained from the remanent magnetization states for various $H_{CF}$.



**Fig. 5.** (*Top panel*) Micromagnetic modeling of the hysteresis loops of FM square (*red curve*) and zero-field cooled FM/AFM square element (*blue curve*). (*Bottom panel*) Simulated hysteresis loop of FM/AFM squares with $H_{CF}=100$ Oe (*red curve*) is compared to ZFC element (*blue curve*). The inset shows the cooling field dependence of $H_{ex}$ (o) and the vortex core position at remanence (□) obtained from modeling. The dotted lines are guides to the eye.

Landau vortex states are compared in the bottom panel of Fig. 4, in which the total energy $E_{tot}$ consists of exchange energy ($E_{ex}$), anisotropy energy ($E_{ani}$), demagnetizing energy ($E_{dem}$), and pinning energy ($E_{pin}$) contributions. In general, the contribution of $E_{dem}$ and $E_{pin}$ to the total energy significantly increases with increasing $H_{CF}$, whereas $E_{ex}$ and $E_{ani}$ remain almost constant. It is noteworthy that the demagnetizing energy $E_{dem}$ counteracts $E_{pin}$, in which $E_{dem}$ strongly increases as the element becomes more magnetized in the $H_{CF}$ direction.

The simulated hysteresis loops for the FM square element (*blue curve*) and the FM/AFM bilayer element with $H_{CF}=0$ Oe (*red curve*) are shown in the top panel of Fig. 5. The results are in a good qualitative agreement with the experimentally observed hysteresis loops in Fig. 1. The modeling reproduces the constricted central portion, the characteristic feature of the vortex-driven magnetization process. The increases in the vortex core annihilation field, $H_A$, as well as the decreases in coercivity, $H_c$, and remanence, $M_R$, for the ZFC element compared to the FM reference are also faithfully reproduced. These results support the assumption that the increase in vortex stability, experimentally observed in Fig. 1(b), is induced by the local effective pinning fields at the FM/AFM interface which originates from the imprinting of the
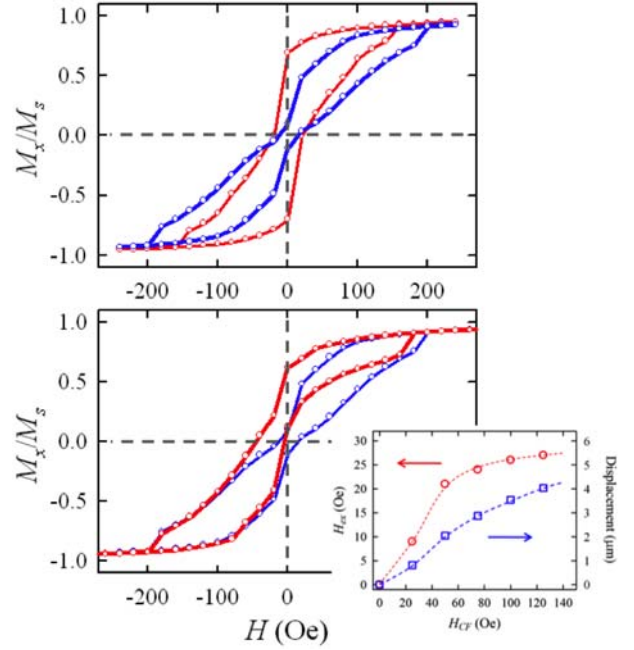
vortex state of FM layer into AFM. Furthermore, the effects of the imprinting of the displaced vortex structure for the field-cooled elements are evident. The bottom panel of Fig. 5 shows the hysteresis curve for the element subject to the local pinning fields with the distribution of the displaced vortex state by applying $H_{CF}$ of 100 Oe (*red curve*), together with the loop for the ZFC element (blue curve). The inset in Fig. 5 shows the cooling field dependence of $H_{ex}$ (o) and the vortex core position at remanence (□) obtained from the modeling. Similar to the experimental result in Fig. 2(e), there is a strong correlation between the displacement of the vortex core and $H_{ex}$. Also noticeable in Fig. 5 (bottom panel) is the asymmetry in the hysteresis shape for FC element (*red curve*), which is induced due to the vortex-shifted asymmetric Landau vortex state, in which the vortex core is far off-center at remanence.

## 4. Conclusions

The effects of the local pinning field on the remanent magnetization configuration and magnetization process in $Ni_{80}Fe_{20}/Ir_{20}Mn_{80}$ square elements have been investigated.

The result demonstrates the possibility to imprint a vortex shifted asymmetric Landau structure into the AFM layer in micron-sized FM/AFM bilayer elements. In ZFC elements, the symmetric exchange-bias geometry provides a low-energy vortex reference state, improving the stability of the symmetric vortex structure. The vortex shift and exchange-bias field are tunable through the choice of cooling field strength. Micromagnetic modeling yields conclusive evidence confirming the experimental observations, in which the exchange-coupling induced local pinning field plays an important role in remanent vortex configuration and magnetization process in $Ni_{80}Fe_{20}/Ir_{20}Mn_{80}$ square elements.

## Acknowledgements

## References

[1] J. Nogués, J. Sort, V. Langlais, V. Skumryev, S. Suriñach, J. S. Muñoz, and M. D. Baró, Phys. Rep. **422**, 65 (2005).

[2] J. Eisenmenger, Z. P. Li, W. Macedo, and I. K. Schuller, Phys. Rev. Lett. **94**, 057203 (2005).

[3] W. Jung, F. J. Castaño, and C. A. Ross, Phys. Rev. Lett. **97**, 247209 (2006).

[4] C. M. Schneider, O. de Haas, D. Tietjen, U. Muschiol, N. Cramer, Z. Celinski, A. Oelsner, M. Klais, C. Zieten, O. Schmidt, G. Schönhense, N. Zema, and S. Zennaro, J. Phys. D **35**, 2472 (2002).

[5] J. Fassbender, S. Poppe, T. Mewes, A. Mougin, B. Hill-ebrands, D. Engel, M. Jung, A. Ehresmann, H. Schmoranzer, G. Faini, K. J. Kirk, and J. N. Chapman, Phys. Status Solidi (a) **189**, 439 (2002).

[6] B. C. Choi, E. Girgis, C. A. Ross, Th. Speliotis, Y. K. Hong, G. Abo, D. Niarchos, and H. Miyagawa, Phys. Rev. B **81**, 092404 (2010).

[7] B. C. Choi, Y. K. Hong, J. Rudge, G. W. Donohoe, and Q. F. Xiao, J. Magnetics **11**, 61 (2006).

[8] J. Sort, K. Buchanan, V. Novosad, A. Hoffmann, G. Salazar-Alvarez, and A. Bollero, Phys. Rev. Lett. **97**, 067201 (2006).

[9] U. Nowak, K.D. Usadel, J. Keller, P. Miltényi, B. Beschoten, and G. Güntherodt, Phys. Rev. B **66**, 014430 (2002).

[10] J. Mejía-López, P. Soto, and D. Altbir, Phys. Rev. B **71**, 104422 (2005).

[11] J. Sort, A. Hoffmann, S.-H. Chung, K. S. Buchanan, M. Grimsditch, M. D. Baró, B. Dieny, and J. Nogués, Phys. Rev. Lett. **95**, 067201 (2005).

[12] J. Sort, G. Salazar-Alvarez, M. D. Baró, B. Dieny, A. Hoffmann, V. Novosad, and J. Nogués, Appl. Phys. Lett. **88**, 042502 (2006).

[13] W. P. Meiklejohn and C. P. Bean, Phys. Rev. **102**, 1413 (1956).

[14] W. P. Meiklejohn and C. P. Bean, Phys. Rev. **105**, 904 (1957).

[15] M. Tanase, A. K. Petford-Long, O. Heinonen, K. S. Buchanan, J. Sort, and J. Nogués, Phys. Rev. B **79**, 014436 (2009).

[16] M. R. Scheinfein, LLG Micromagnetics Simulator™, Version 2.63c (2009).

[17] C. Leighton, J. Nogués, H. Suhl, and I. K. Schuller, Phys. Rev. B **60**, 12837 (1999).

[18] E. D. Dahlberg, B. Miller, B. Hill, B. J. Jonsson, V. Strom, K. Rao, J. Nogues, and I. K. Schuller, J. Appl. Phys. **83**, 6893 (1998).